Heterogeneity of sea ice surface temperature at SHEBA from aircraft measurements

Julie A. Haggerty,[1] James A. Maslanik, and Judith A. Curry[2]
Program in Atmospheric and Oceanic Sciences, University of Colorado, Boulder, Colorado, USA

Received 19 July 2000; revised 3 December 2002; accepted 17 June 2003; published 31 October 2003.

[1] Large variations in surface temperature of sea ice occur on a seasonal scale, and spatial variations are also significant due to exposure of open water in leads and varying thickness of sea ice. In this paper we examine aircraft, ground-based, and satellite measurements of sea ice surface temperature over the region surrounding the Surface Heat Budget of the Arctic Ocean (SHEBA) ice station. Aircraft measurements from May and July demonstrate the spatial and temporal variability of surface temperature for the consolidated ice pack and for leads over the local area (which is defined here as the 30 $\times$ 30 km square observed by the aircraft). Data from May show a large increase in surface temperature during the month, but spatial variability of the thick ice temperature over the local area is not large with standard deviations on the order of 0.5 K. Surface temperatures during the melt season (July) were more uniform and near freezing as expected. Standard deviations during this period are smaller than in spring. Our analysis shows that surface temperature at a point (the SHEBA ice station) approximates the mean value over the local area during late spring and summer with an RMS error of 0.75 K. Lead temperatures cannot be reliably represented by the point measurements at the ice station. Surface temperature retrievals from advanced very high resolution radar (AVHRR) were compared with aircraft and ground-based measurements in late May. Mean surface temperature values over the local area as derived from AVHRR and aircraft measurements were within 1.5 K of each other. Mean surface temperatures over varying spatial scales were calculated and found to differ by as much as 1.3 K from local to regional scales (500 km) in late May. *INDEX TERMS:* 3349 Meteorology and Atmospheric Dynamics: Polar meteorology; 9315 Information Related to Geographic Region: Arctic region; 4275 Oceanography: General: Remote sensing and electromagnetic processes (0689); *KEYWORDS:* sea ice, surface temperature, aircraft measurements, spatial variability

Citation: Haggerty, J. A., J. A. Maslanik, and J. A. Curry, Heterogeneity of sea ice surface temperature at SHEBA from aircraft measurements, *J. Geophys. Res.*, *108*(C10), 8052, doi:10.1029/2000JC000560, 2003.

1. Introduction

[2] Sea ice surface temperature affects the rate of sea ice growth, snow metamorphosis, and snow and ice melt processes. Parameterization of radiative and turbulent heat fluxes between the sea ice and the atmosphere require accurate measurement of surface temperature and the surface-air temperature difference. Satellite retrievals of cloud and surface properties (e.g., sea ice type) rely on estimates of surface temperature. Large variations in surface temperature of sea ice occur on a seasonal scale, and spatial variations are also significant due to exposure of open water in leads and varying thickness of sea ice.

[3] While it is known that the consolidated ice pack exhibits significant spatial inhomogeneity in various physical properties including surface temperature, there is little information available documenting small-scale fluctuations in surface temperature over large regions. Surface-based measurements during the Surface Heat Budget of the Arctic Ocean (SHEBA) experiment provide high frequency time series of surface temperatures for multiyear ice over a yearlong measurement period, but only at a few closely spaced points around the SHEBA ice station [*Claffey et al.*, 1999]. Lead surface temperatures were also measured in a single lead near the SHEBA site during summer [*Pegau and Paulson*, 1999] and by *Maslanik et al.* [1999] on a few days in spring. Methods for deriving surface temperature in polar regions from satellite sensors such as AVHRR [*Key et al.*, 1997] expand spatial coverage, but the resolution is often too coarse to isolate small-scale variations such as those caused by subpixel scale leads or to resolve variations within leads. In addition, clouds frequently obscure the surface from observation by satellite, limiting the frequency and/or accuracy with which surface temperature can be retrieved. Aircraft platforms provide high-resolution measurements of surface temperature over an area larger than that observed by

[1] Now at National Center for Atmospheric Research, Boulder, Colorado, USA.
[2] Now at Georgia Insitute of Technology, Atlanta, Georgia, USA.

0148-0227/03/2000JC000560$09.00

the ground-based sensors. Although limited to specific time periods during SHEBA, the aircraft data set allows us to quantify the spatial heterogeneity over the region, monitor the evolution of surface temperature through the spring and summer seasons, and characterize temperature variations within leads. Thus we can use the aircraft data to bridge a gap between point measurements at the ice station and satellite retrievals. From these analyses, we can assess how representative the ice station measurements are of the surrounding area as well as how representative the SHEBA area is of the larger region. Specifically, we address the following objectives in this paper:

[4] 1. Compile statistics that describe the spatial and temporal variability of the ice pack surface temperature in the local area observed by the aircraft during spring and summer.

[5] 2. Compare mean values of surface temperature in the local area with ground-based measurements at the SHEBA station to ascertain how well point measurements represent the aggregate scale.

[6] 3. Compare aircraft measurements with AVHRR surface temperature estimates to assess the accuracy of the satellite retrieval method. Determine the variability of surface temperature as a function of spatial scale.

2. Data Set

[7] The SHEBA field experiment was conducted from October 1997 to October 1998 in the Beaufort and Chukchi Seas [*Perovich et al.*, 1999]. The Canadian Coast Guard icebreaker Des Groseilliers served as a base camp to deploy a variety of sensors that measured ice, snow, and meteorological properties. In conjunction with the SHEBA effort, the FIRE Arctic Clouds Experiment extended the spatial domain of the experiment with aircraft observations of atmospheric and surface properties in the vicinity of the Des Groseilliers [*Curry et al.*, 2000].

[8] Aircraft measurements around the SHEBA ice station were conducted in the spring and summer of 1998. The National Center for Atmospheric Research (NCAR) C-130 performed 8 research flights in May and 8 in July of that year. Surface (skin) temperature was measured remotely from the aircraft by a set of two Heimann Model KT19.85 pyrometers [*Research Aviation Facility* (*RAF*), 1994]. Flight patterns were designed to sample a grid space centered on the SHEBA ice station, typically covering an area of 30 $\times$ 30 km.

[9] The Heimann radiometers detect radiation within the spectral range 9.6–11.5 μm over a 2° field of view (FOV). Absolute accuracy of the sensors is ±0.5°C plus 0.7% of the difference between the sensor housing temperature and scene temperature. During FIRE-SHEBA, the sensor was maintained at 286–290 K, while the lowest scene temperatures observed were on the order of 257 K. In the worst case, the specified error is then 0.73 K. Data were sampled at 5 Hz, so given a nominal aircraft speed of 100 m s^{-1}, a data point is available every 20 m. The C-130 operated at altitudes ranging from 30 m to 4000 m above the surface, so resulting pixel sizes are approximately 1 m to 140 m. In section 3, a method is presented for retrieving surface temperature from KT19 measurements of brightness temperature.

[10] Surface temperature at the SHEBA ice station was also estimated from measurements by two sets of downward and upward looking Eppley pyrgeometers [*Claffey et al.*, 1999]. The data analyzed in this paper are hourly averages compiled from surface-based measurements taken near the main flux tower. *Claffey et al.* [1999] found good agreement between the two sets of Eppley sensors.

[11] Surface-based measurements of surface and air temperature over various ice types were acquired using a mobile radiometric platform (MRP). The MRP included a KT19 infrared pyrometer and shielded thermistor. During April through early May, measurements were made at the edges of several leads [*Maslanik et al.*, 1999]. *Pegau and Paulson* [1999] measured near-surface temperature in a lead about 1 km from the SHEBA ice station from 7 June to 8 August 1998 using a SeaBird SBE-19 conductivity-temperature-pressure (CTD) sensor mounted on the underside of a small boat.

[12] Finally, surface temperature estimates derived from AVHRR radiances are available during the experimental period from the NOAA/NASA AVHRR Polar Pathfinder Project. The method for relating satellite radiances to surface temperature is based on model simulations of sensor radiances using Arctic and Antarctic radiosonde data as input [*Key et al.*, 1997; *Maslanik et al.*, 2001]. Empirical formulae developed from the model results are used to estimate surface temperature from 11 and 12 μm brightness temperatures, assumed surface emissivities, and satellite viewing angle. Reported accuracies are in the range of 0.3–2.1 K. *Key et al.* [1997] attribute the larger errors to spatial heterogeneity of the surface. Errors are also thought to result from deficiencies in cloud-masking algorithms used in the method [*Maslanik et al.*, 2001].

3. Data Processing and Analysis Procedures

[13] Flights with useful measurements of surface temperature were conducted on six dates during May and four dates during July. In each of these cases, the aircraft was able to fly below the cloud base or skies were clear, so an unobstructed view of the surface was available for at least part of the flight. Flight patterns centered on the ice station and typically covered a square 30 km on each side. Flight altitudes were typically below 1500 m.

[14] Following identification of cloud-free data segments, KT19 brightness temperatures were converted to corresponding surface temperatures. The observed brightness temperature at the aircraft is comprised of contributions from surface emission, direct atmospheric radiance, and reflected atmospheric radiance. Mathematically, the radiance at a given frequency, ν, observed at the top of a nonscattering, plane parallel atmospheric layer can be expressed as [*Liou*, 1980]:

$$L_m = \varepsilon_\nu L_{sfc} + L_{atm} + (1 - \varepsilon_\nu) L_{ref}, \quad (1)$$

where L_m is measured upwelling radiance at the top of the layer, ε_ν is the emissivity of the surface at the given wavelength, and L_{sfc} is the surface radiance given by:

$$L_{sfc} = B_\nu(T_s)\tau(p_s, p_0). \quad (2)$$

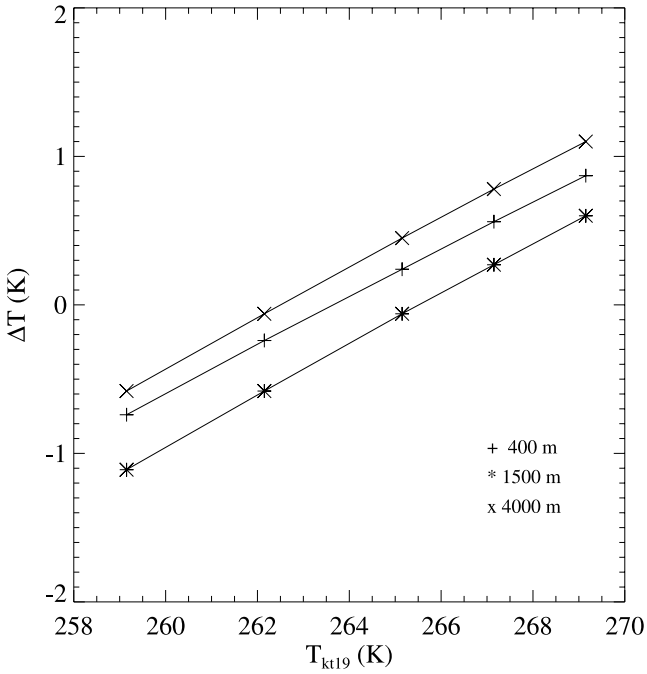

Figure 1. Corrections applied to KT19 brightness temperature measurements to account for atmospheric radiance and emissivity effects. Data shown are for 20 May 1998 at three flight altitudes.

Here B_ν is the Planck function, T_s is surface temperature, τ is atmospheric transmittance, and p_s and p_0 are pressure at the surface and top of the layer, respectively. L_{atm} is direct atmospheric radiance given by:

$$L_{atm} = \int_{p_s}^{p_0} B_\nu[T(p)] \frac{\partial}{\partial p} \tau(p, p_0) dp, \tag{3}$$

and L_{ref} is atmospheric radiance reflected by a nonblackbody surface:

$$L_{ref} = [\tau(p_s, p_0)]^2 \int_{p_s}^{p_0} \frac{B_\nu[T(p)]}{[\tau(p, p_0)]^2} \frac{\partial}{\partial p} \tau(p, p_0) dp. \tag{4}$$

Rearranging (1) and substituting from (2)–(4), we can solve for surface temperature as:

$$T_s = B_\nu{}^{-1} \left(\frac{L_m - L_{atm} - (1 - \varepsilon_\nu) L_{ref}}{\varepsilon_\nu \tau(p_s, p_0)} \right), \tag{5}$$

where $B_\nu{}^{-1}$ is the inverse of the Planck function. Given measurements of L_m from the KT19 along with vertical profiles of temperature and humidity, we can calculate the terms in (5) to arrive at an estimate of surface temperature.

[15] Similar corrections have been previously applied to infrared temperature measurements of sea ice by *Steffen and Lewis* [1988] and *Muller et al.* [1975]. Following their methods, we use a radiative transfer model [*Key and Schweiger*, 1998] to calculate the differences between brightness temperature and surface temperature for each of the days analyzed here. Temperature and humidity profiles acquired during the aircraft flights were used with the model to ascertain the effects of absorption and emission by atmospheric water vapor. Calculations were performed over the spectral band observed by the KT19 using the appropriate weighting function. The effect of varying infrared emissivity was also considered with these model runs. The actual emissivity depends on many factors (e.g., snow grain size, extent of melting) that cannot be characterized from the available data [*Salisbury et al.*, 1994]. For consistency with emissivity values used in analysis of surface-based temperature measurements [*Claffey et al.*, 1999], we assume $\varepsilon_\nu = 0.99$. This value is also a good approximation for the emissivity of open water in this spectral range [*Muller et al.*, 1975].

[16] Model runs were performed over a range of hypothetical surface temperatures. The differences between model estimates of infrared brightness temperature at flight altitude and the input surface temperature give the correction to be applied. Temperature corrections on a given day are a function of flight altitude and observed brightness temperature. Figure 1 shows corrections at typical flight altitudes for 20 May 1998. Least squares fits to the model output are shown; these curves are used to "look up" the appropriate correction for a given brightness temperature and flight altitude. An example illustrating the effect of the corrections on 20 May 1998 is given in Table 1. On this clear and fairly dry day, adjustments on the order of 0.4 K were applied to the raw KT19 data. Comparison with ground-based measurements at the SHEBA ice station demonstrate that the corrected temperatures more closely match the Eppley data than do measured brightness temperatures.

[17] Each pixel in the resulting data set was then classified as containing either lead (open water or thin ice) or thick, white ice based on a subjectively determined temperature threshold. Initial estimates of the threshold for each flight were assessed by comparing resulting lead fractions to those obtained by viewing images from the C-130s downward looking video camera. Temperature thresholds were adjusted until lead fractions estimated from each source were in agreement.

4. Results

4.1. Temporal Variability of Surface Temperature

[18] The variations in surface temperature along flight segments near the SHEBA ice station are shown in Figure 2. Each of the segments is oriented east-west, approximately 30 km in length, and is measured from an altitude of about 100 m (so resolution is the same in all cases). The trace for 7 May shows a clear separation between temperatures of newly frozen ice and open water in leads and the surround-

Table 1. Effect of Atmospheric and Surface Emissivity Corrections on KT19 Data at the SHEBA Site for 18 May 1998

Time, UTC	Flight Altitude, m	Uncorrected KT19 Temperature, K	Corrected KT19 Temperature, K	Eppley Temperature, K
2129	4000	263.9	264.3	264.9
2204	1500	264.8	265.2	265.2
2311	400	265.1	265.4	265.5

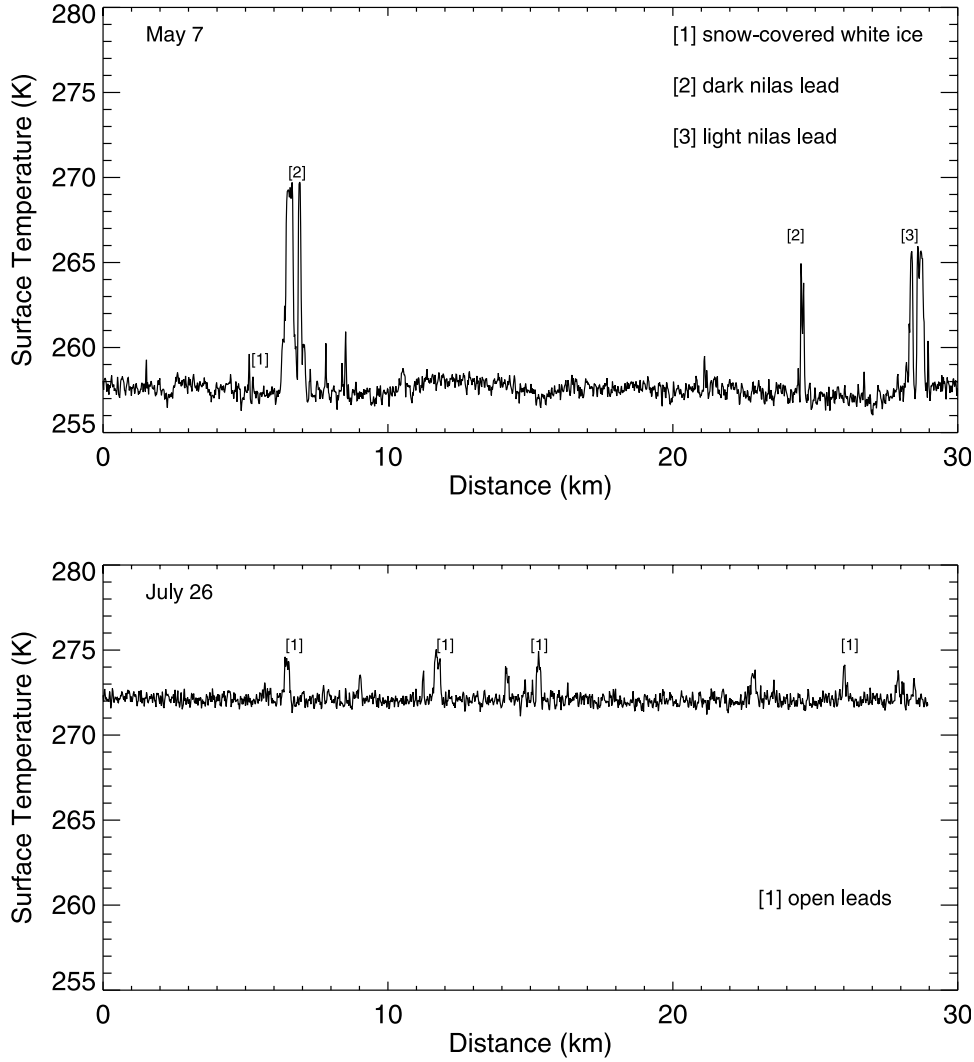

Figure 2. Surface temperature along flight tracks near the SHEBA ice station on 7 May and 26 July 1998. Ice types as inferred from video tape are indicated for selected temperature features.

ing thick, white ice. While thick ice temperatures fluctuate about 257–258 K, temperatures of thin ice within the leads are at least 2–3 K warmer. Three large leads are detected at approximately 7 km, 25 km, and 28 km from the beginning of the flight segment with temperatures in excess of 265 K. Visual observations of these leads suggest that areas of open water and thin nilas were present. Since observed temperatures were significantly lower than that expected for open water, the scale of the open water areas is assumed to be subpixel size and/or small enough to fall between samples which are separated by approximately 20 m. The effect of these sampling limitations is, as expected, significant for small leads. For example, MRP observations at a newly opened lead of approximately 18 m width showed surface temperatures within the lead of about 269 K. Concurrent C-130 overflights of the lead were conducted perpendicular to the lead's axis. The lead was uniformly covered by about 5 cm of congelation ice, with some frost flowers present. Owing to the sampling rate and FOV of the KT19, the maximum surface temperature observed in this relatively small lead from the C-130 was only 261 K. A parallel track over the lead resulted in a C-130 temperature of 264 K. Surface temperatures of the adjacent thick ice were typically within 0.5 K of that measured by the C-130.

[19] In early July the surface is melting and temperatures are at or just above freezing. Surface temperatures of open water in leads and thick, white ice are nearly the same. Later in the month (26 July), Figure 2 shows that the background temperature remains near freezing, but lead temperatures have increased by 1–2 K and are now easily distinguished from the thick, white ice signature. Lead surface temperature increased throughout July due to radiative absorption by the water in conjunction with weak vertical mixing. This pattern is consistent with the *Pegau and Paulson* [1999] in situ observations of a lead near the ice station, and was also noted in AVHRR data by *Maslanik et al.* [2001].

[20] Mean surface temperatures for each flight in May are plotted in Figure 3 with the time series of point measurements from the SHEBA ice station superimposed. During the first week in May, the mean temperature begins at about 260 K on 4 May, then decreases by approximately 2 K on 7 May (see Table 2) as did the surface air temperature during that period. Average lead temperatures increased slightly to about 261 K as more open water was exposed

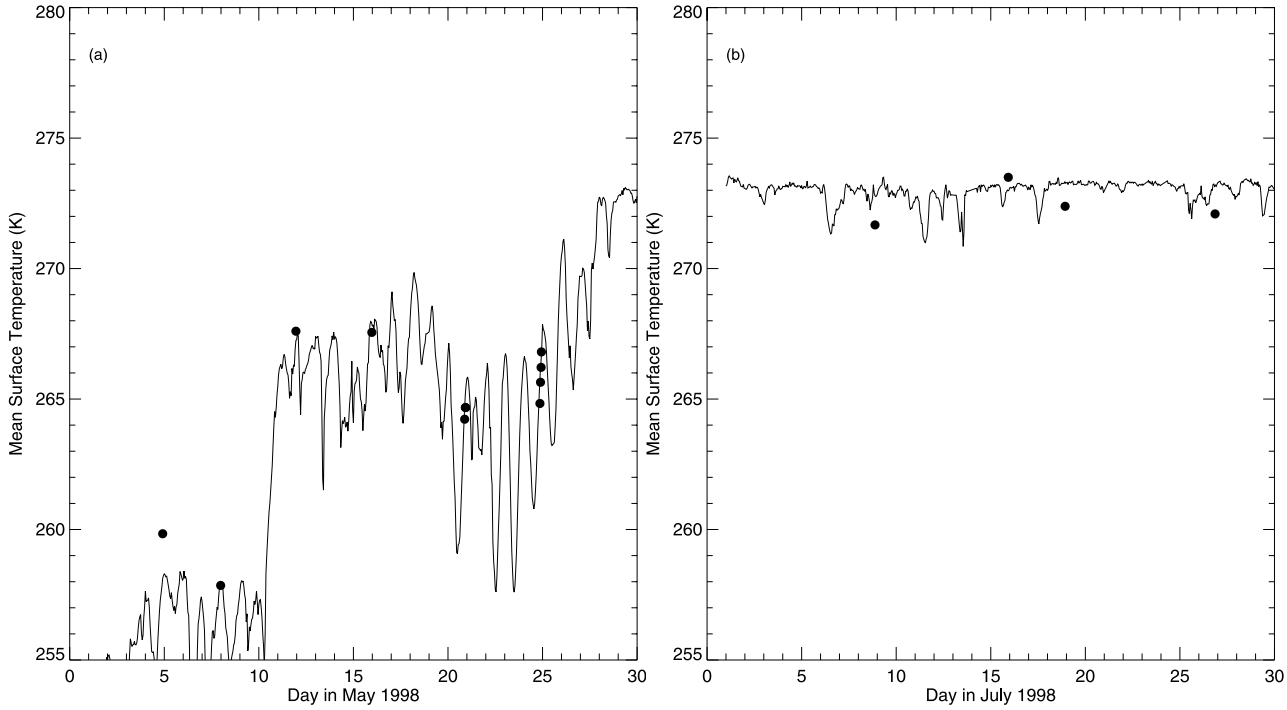

Figure 3. Mean surface temperature at SHEBA ice station (solid lines) with aircraft average (points) superimposed during May and July 1998.

by ice divergence between 4 and 7 May (Table 3). Significant increases in temperature due to southerly winds occurred in the second week of May. Ice pack mean temperatures on 11 and 15 May were 267–268 K, an increase of almost 10 K from the previous week. Similar increases in near-surface air temperatures were observed. Mean temperatures of leads also increased considerably to about 269 K. During the third week in May, a high-pressure system resulted in clear skies on two of the flight days. Radiative losses produced cooling at the surface, and we see lower mean temperatures of 265–267 K. Mean lead temperatures fell by 2–3 K.

[21] Figure 3 also shows mean temperatures for the area around the ice station in July as calculated from aircraft data with ground-based measurements from the ice station superimposed. We first note that low clouds obscured our view of the surface more frequently in July than in May, so fewer data points are available. The four flight days on which useful data are available show small variations in temperature, consistent with the melted state of the surface. As noted previously, leads were not discernible in the temperature data during the first part of July, but differences became apparent during the second half of the month as the lead surface temperatures increased. Since the entire surface is near freezing, lead surface temperatures are higher than the adjacent thick ice by only 1–2 K (Table 3).

4.2. Data Comparisons

[22] Figure 4 is a scatterplot showing the correlation between ground-based measurements from the Eppley sensors with KT19 measurements for the pixel nearest the ice station. Note that the KT19 measurements are taken at different altitudes, so the field of view for each point may be different and certainly encompasses more area than the Eppley sensors are viewing. The comparison shows reasonably good agreement considering the differing fields of view and the accuracies of each sensor. The correlation coefficient is 0.986 and RMS error is 0.75 K. Physical air temperatures (at 12 cm) measured at the ice station are found to be 0.2–1 K higher than the surface temperature obtained from the Eppley sensors, but still correlate well with the KT19 measurements.

[23] Similarly, we compare aircraft and ground-based measurements with AVHRR estimates of surface temperature for available passes of NOAA-14. Table 4 lists mean values over the area observed by the aircraft as calculated from AVHRR retrievals [*Maslanik et al.*, 2001] and KT19 measurements during clear sky conditions. The differences of 0.2 and 1.5 K between the satellite and aircraft estimate are within the error range specified for the AVHRR surface temperature retrieval method. Table 5 compares AVHRR estimates at the pixel including the ice station to the Eppley

Table 2. Summary of Surface Temperature Data for Pack Ice in the Aircraft Sampling Region Around SHEBA

Date in 1998	Mean Temperature, K	Standard Deviation, K
4 May	259.8	0.57
7 May	257.9	1.427
11 May	267.6	0.697
15 May	267.6	0.79
20 May	264.2	0.62
24 May	264.8	0.50
8 July	271.7	0.34
15 July	273.5	0.39
18 July	272.4	0.32
26 July	272.1	0.37

Table 3. Summary of Surface Temperature Data for Newly Frozen Ice and Open Water Within Leads in the Aircraft Sampling Region Around SHEBA

Date in 1998	Mean Temperature, K	Standard Deviation, K
4 May	261.0	0.50
7 May	261.2	2.61
11 May	269.2	0.66
15 May	269.0	0.75
20 May	265.7	0.77
24 May	266.2	0.64
18 July	273.5	0.61
26 July	273.5	0.56

surface temperature measurements at the ice station. There are differences of about 2 K in both cases. Larger differences from this comparison are not unexpected considering that the satellite pixel encompasses an area of 5 km on a side while the ground-based sensor gives a point measurement.

4.3. Spatial Variability as Estimated From Aircraft Data

[24] Figure 5 shows the area fraction occupied by a given surface temperature over the aircraft observation area for three dates during the experiment. In all cases the variation in temperature is modest, with over 50% of the area having temperatures within ±0.5 K of the mean, and at least 90% of the area within ±1 K of the mean. Standard deviations in surface temperature over the 30 km boxes are given in Tables 2 and 3. The standard deviation for the ice pack (including thick, white ice, ridges, and leads) is fairly constant throughout May with the exception of 7 May. Variability in surface temperature over thick ice and snow covered leads was negligible as measured by the MRP in April and early May. Point measurements of surface temperature over ridges from the MRP showed typical variations of 2–4 K under overcast conditions, and about twice as large during clear-sky conditions. As expected, variability in lead temperatures is greater than in the surrounding thick ice with standard deviations varying from 0.5–2.6 K (Table 3). The 7 May case shows the largest variability in lead temperature due to the higher fraction of open water and new ice leads observed on that day. As noted earlier, this range is an underestimate of true conditions during cold periods due to the sizes of ridges and open areas in leads compared to the FOV of the aircraft mounted KT19. Variations are smaller in July when melt conditions caused most surface features to have nearly the same temperature. Standard deviations are on the order of 0.3–0.4 K. Lead temperatures still exhibit more variability than the thick, white ice, but not as much variability as in the leads observed during May.

[25] One of the objectives of this work is to determine how well a point measurement of surface temperature represents the average temperature over the area observed by the aircraft. Figure 6 indicates that the area-mean surface temperature (excluding leads) is highly correlated with the one-pixel surface temperature measured at the SHEBA ice station for the ensemble represented by the series of May and July flight tracks. This high correlation is explained by the fact that spatial standard deviations of surface temperature are small compared to the predominantly seasonal

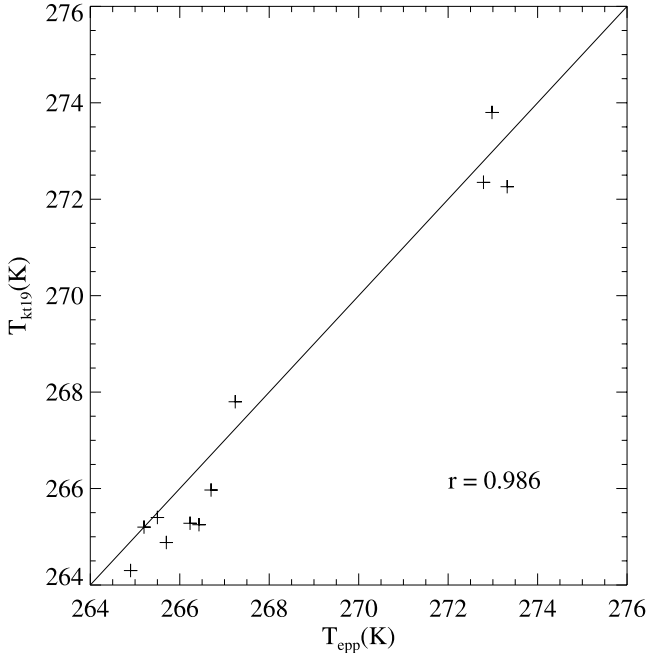

Figure 4. Comparison of surface temperature derived from the KT19 with ground-based Eppley measurements for cases where the C-130 overflew the SHEBA ice station.

variations of temperature among the different flights. It should be noted, however, that conditions in May 1998 were warmer than usual and the ice pack was less active dynamically, so temperature variation may have been smaller than in a more typical year.

[26] The data set was also examined for spatial gradients over the region surrounding the ice station. Northward and eastward components of the horizontal temperature gradient were estimated for each flight using least squares linear regression to fit measured temperature to latitude and longitude, respectively. Largest gradients were found on 20 May when surface temperature increased by 0.5 K per 50 km northward and eastward. Even these largest gradients are comparable to or less than the measurement uncertainty of the KT19 sensor. Temporal variations during the flights introduce additional uncertainties of similar size. Hence the only conclusion apparent from this analysis is that the magnitude of the actual surface temperature gradient is probably smaller than 0.5 K per 50 km.

[27] Smaller-scale variability and the relationship between temperatures at points separated by a specified distance were analyzed by calculating the semivariance. Semivariance is the expected value of the squared difference between two observations separated by some distance [*Davis*, 1986]. Figure 7 gives the semivariance of surface

Table 4. Mean Surface Temperatures and Standard Deviations From Satellite Retrievals Versus Aircraft Measurements Over a 50 × 30 km Area

Date in 1998	T_{avhrr}, K	T_{kt19}, K
20 May	264.9 (0.96)	264.7 (0.58)
24 May	268.3 (0.27)	266.8 (0.6)

Table 5. Surface Temperature From Satellite Retrievals Versus Ground-Based Measurements at the SHEBA Ice Station

Date in 1998	T_{avhrr}, K	T_{eppley}, K
20 May	264.9	267.1
24 May	268.2	266.5

temperature as a function of spatial separation. Data show that the variance of the difference in temperature at two points increases with spatial separation up to several hundred meters. The semivariance levels off at spatial separations above 700 m. *Lindsay et al.* [1996] similarly found that the majority of the variances in skin temperature occurred over a distance of about 800 m or less. These results suggest that optimum spatial resolution for remote sensing of skin temperatures is substantially less than 1 km, if the objective is to obtain representative lead temperatures by minimizing the effects of mixed pixels.

[28] On select flights, the C-130 flew along large leads at low altitude, providing an uncontaminated measure of lead surface temperature and variability. Figure 8 shows surface temperature along one such flight track on 7 May. The lead sampled on 7 May had large variations in surface temperature with minima near 258 K and maxima at 270 K. Ice types as inferred from video tape are associated with notable surface temperature features in Figure 8. In situ observations of this lead (J. Pinto, private communication, 2001) note frazil ice production and open water in the center of this lead with relatively thick ice near the edges.

[29] When comparing the statistics for these individual leads with those for all leads observed during the large-scale flight patterns, we note that the mean and standard deviation are higher when the sensor is viewing leads exclusively. For instance, on 7 May the mean temperature for the single lead shown in Figure 8 is 1.6 K higher than the mean for all leads in the sampling area (see Table 3). The standard deviation is higher by 0.27 K for this case. Since many leads are not large enough to occupy an entire KT19 pixel when the aircraft is conducting large-scale flight patterns at an altitude

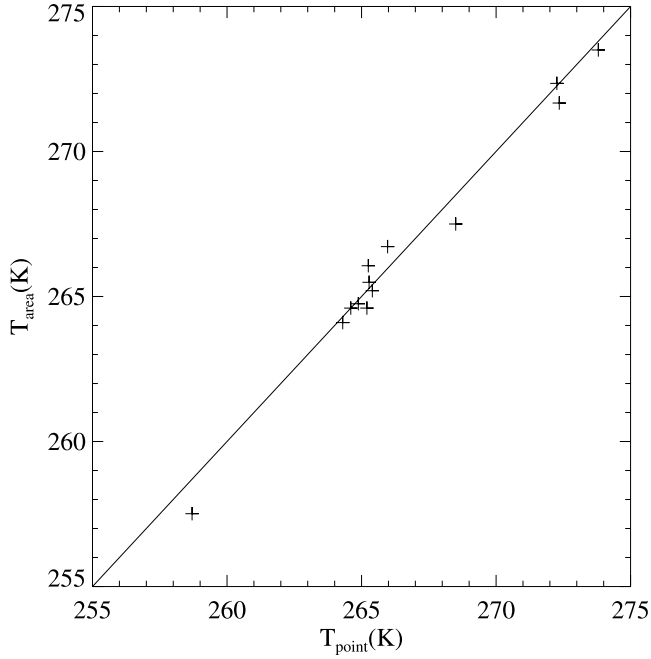

Figure 6. Comparison of KT19 surface temperatures at the SHEBA site (“point” measurement) with mean values over the C-130 flight patterns (“area” measurement).

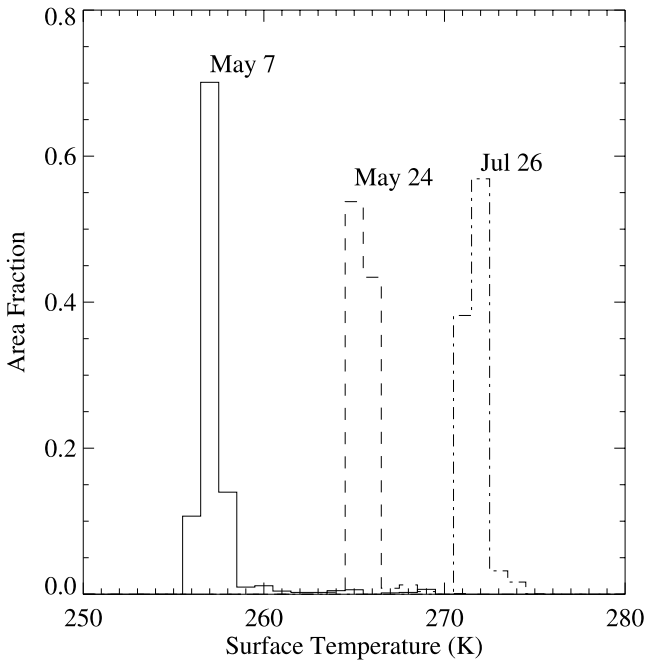

Figure 5. Distribution of surface temperatures over a 30 km box surrounding the SHEBA ice station for 7 and 24 May and 26 July 1998.

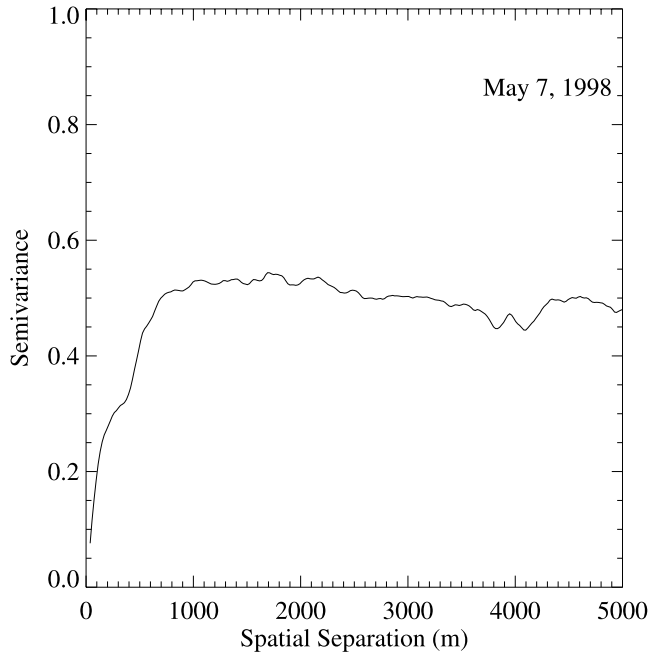

Figure 7. Semivariogram for surface temperature over the area around the SHEBA ice station. The semivariance is the variance of the difference between temperature values separated by a specified distance as given on the *x* axis.

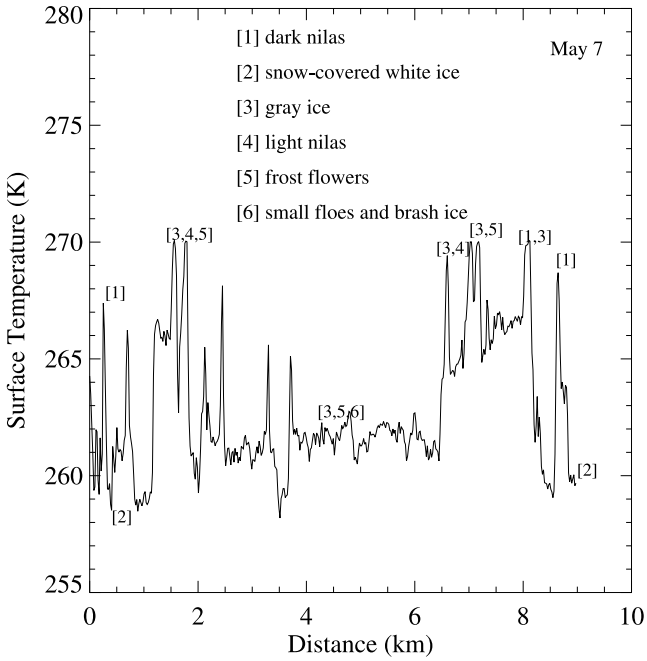

Figure 8. Surface temperature variation along a lead on 7 May 1998. Ice types as inferred from video tape are indicated for selected temperature features.

of 1500 m, contamination by thick ice causes underestimation of the lead temperature and reduces the observed variability.

[30] Finally, the aircraft measurements were analyzed to determine typical spacing between leads as represented by temperature features in the times series data. Visual examination of the surface temperature data demonstrated that features with temperatures approximately 1 K above the mean temperature were generally distinguishable as leads during the May flights. The frequency distribution of distance between 1 K temperature spikes was compiled and is shown in Figure 9. Results show that more than half of the leads are separated by distances of 0.5 km or less, confirming the result suggested by the semivariance analysis that fine-resolution data is required to discriminate leads from thicker, colder ice in a manner that provides accurate lead temperatures. The remaining leads are separated by distances of up to 10 km. Analysis of spacing between leads with higher temperatures (defined as features with temperatures 2 K and 3 K above the mean temperature) suggest that distances between these leads are generally larger than is the case for all leads (as defined by the 1 K threshold), but available data do not provide sufficient sample sizes to draw a definitive conclusion.

4.4. Spatial Variability as Estimated From Satellite Data

[31] Although the aircraft measurements of surface temperature provide the most detailed measure of horizontal variability over the local scale, they are available only at sporadic times over a limited period of the year. Thus most applications requiring surface temperature as input will rely on point measurements and/or satellite estimates. In this section, we estimate variability in surface temperature over a range of spatial scales. Using aircraft data we can characterize variability over the local area around SHEBA (up to scales of 30 km), but many applications require estimates of surface temperature over a larger area. Thus we need to understand how well point measurements and satellite data can represent the surface temperature over areas the size of: (1) a single column grid cell (60 × 60 km); (2) a GCM grid cell (250 × 250 km); and (3) the SHEBA region (500 × 500 km).

[32] We demonstrated in section 4.3 that a single KT19 point measurement of surface temperature at the ice station represents the mean value over the observation area (30 × 30 km) with an RMS error less than 0.5 K (see Figure 6). Given the high correlation between the KT19 measurements and Eppley point measurements (Figure 4), we conclude that the surface-based temperature measurements from the Eppley sensors also provide a similarly good estimate for the mean temperature of the pack ice over the aircraft observation area.

[33] AVHRR-derived surface temperatures provide information at larger scales. Figure 10 gives mean surface temperature and normalized standard deviation as a function of spatial scale for areas centered on the SHEBA ice station on two dates in May. Normalized standard deviation is obtained by dividing each standard deviation value by the maximum standard deviation for that case. From the local scale (30 × 30 km) to the regional scale (500 × 500 km), we see changes in the mean surface temperature of 1.3 K on 20 May and 0.6 K on 24 May. Variability as indicated by normalized standard deviation increases with scale in both cases, but is larger on 20 May. The sky was clear over the SHEBA ice station on both of these dates, but satellite imagery indicates that cloud cover was variable over the region on 20 May and the days prior. Clearing continued in

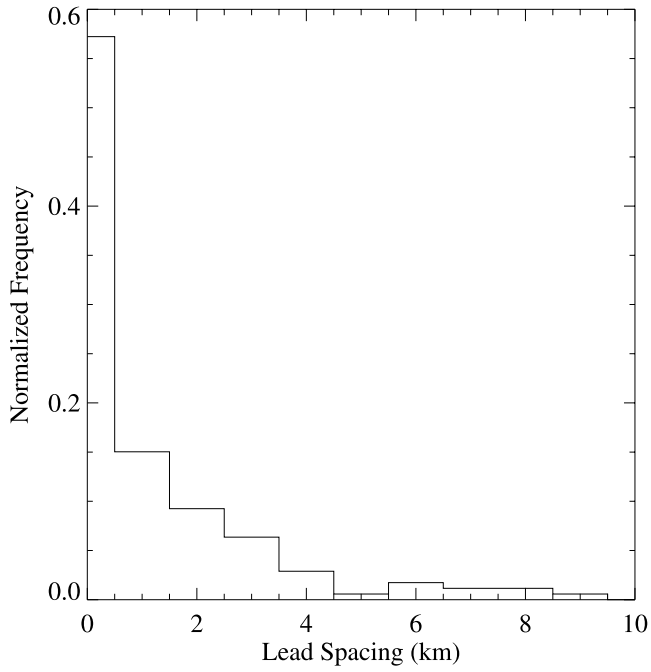

Figure 9. Distribution of distance between leads (defined for this analysis as temperature spikes of at least 1 K above the mean surface temperature) for May 1998.

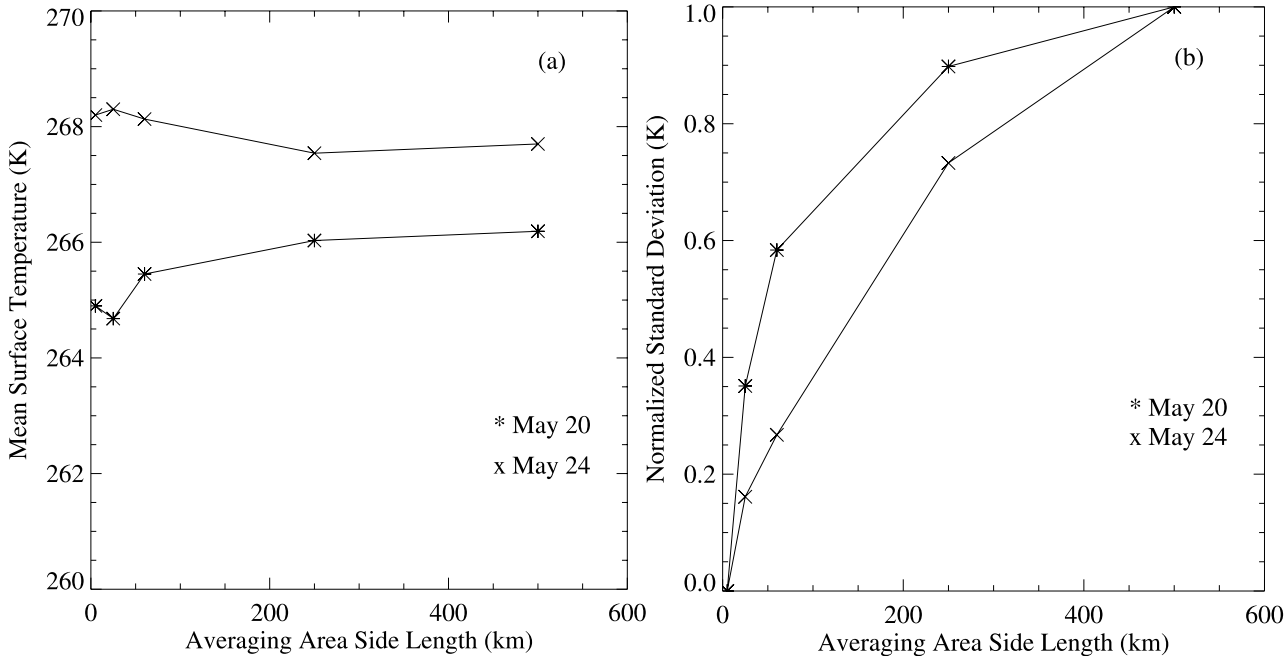

Figure 10. (a) Mean surface temperatures from AVHRR retrievals over varying spatial scales for 20 and 24 May; (b) Normalized standard deviation for the same cases. Normalized standard deviation is obtained by dividing each value by the maximum standard deviation.

subsequent days and the region was entirely clear by 24 May. As noted by *Lindsay and Rothrock* [1994], largest gradients are observed when portions of the surface are under clear skies, and therefore exposed to radiational cooling, while other areas remain cloud covered. Such a situation appears to have existed on 20 May, thereby probably explaining the higher standard deviation compared to 24 May when the sky was clear over a larger region.

[34] Comparison of the single pixel (5 km) and the local scale (30 × 30 km) surface temperatures in Figure 9 confirms our earlier conclusion that a point measurement approximates the local area mean temperature to within 0.5 K at this time of year. Larger differences are apparent between mean surface temperatures over the larger scales. For example, there is a difference of about 1 K between the single column grid cell scale (60 × 60 km) and the GCM grid cell scale (250 × 250 km) on 20 May.

5. Summary and Conclusions

[35] In this paper, we have presented and analyzed measurements of sea ice surface temperature over the region surrounding the SHEBA ice station. The aircraft measurements from May and July have been summarized to demonstrate the spatial and temporal variability of surface temperature for the consolidated ice pack and for leads. Results have been compared to surface temperature measurements derived from ground-based sensors at the ice station and with satellite estimates.

[36] Data from May show a large increase in surface temperature during the second week of the month, and then a slight decrease in temperature during the third week when skies cleared. Spatial variability of the pack ice temperatures is not large with standard deviations on the order of 0.5 K and temperature over most of the local area falling within ±1 K of the mean. Surface temperatures during the melt season (July) were even more uniform and near freezing as expected. Standard deviations during this period are smaller than in spring.

[37] Lead surface temperatures in May are affected by opening and refreezing of the surface which causes large spatial and temporal variations in surface temperature. In early May, differences between lead and pack ice temperatures were as much as 12 K when large fractions of open water were observed. In general, the difference declined over the month as the pack ice temperature increased. Spatial variability of surface temperature within a given lead was found to be large, particularly when open water was present. During the first half of May, standard deviations in lead surface temperatures varied from 1.09–2.87 K. Mean temperatures in leads increased by about 8 K during the month. Data from the summer melt season (July) show that leads were difficult to distinguish early in the month because temperatures were quite similar to the ponded ice. As absorption of radiation increased the temperature of the open water leads and weak mixing limited distribution of the absorbed energy, the lead temperatures rose 1–2 K above the surrounding ice.

[38] Our results show that the surface temperature at a point (the SHEBA ice station) is a good estimate of the mean value over the area sampled by the aircraft during late spring and summer. The correlation between surface temperature at the ice station (as measured by the airborne KT19 sensor) and the mean temperature of the pack ice over the area is 0.99. Standard deviations over the area are comparable to the measurement uncertainty of the sensor. Thus we conclude that using a point measurement in applications that require surface temperature of the local

area (30 × 30 km) is accurate to approximately 0.5 K according to this data set, but may not be as accurate during winter or during a spring season when ice dynamics are more vigorous. We also demonstrated that the ground-based Eppley sensor compares well with the airborne KT19 (i.e., the time series of surface temperature at the ice station provides an estimate for the mean surface temperature over the local area with an RMS error of 0.75 K). Obviously lead temperatures may be considerably different and cannot be reliably represented by the point measurements at the ice station that were obtained over thick ice.

[39] Surface temperature retrievals from AVHRR were compared with aircraft and ground-based measurements in late May. Means over the local area (30 × 30 km) as derived from AVHRR and aircraft measurements differed by 0.2 and 1.5 K for the two cases examined. Point measurements at the ice station differed by about 2 K from AVHRR retrievals for a 5 km pixel containing the ice station. Mean surface temperatures over varying spatial scales were calculated and found to differ by as much as 1.3 K from local to regional scales in late May, and variability increased from small to large scales.

[40] **Acknowledgments.** This research was supported by the NSF SHEBA program, the NASA FIRE program, and a NASA Earth System Science Fellowship. We thank K. Laursen of the NCAR Research Aviation Facility for providing the high rate surface temperature measurements. NOAA Polar Pathfinder data were obtained from the National Snow and Ice Data Center. Robert Stone (CIRES/NOAA) designed and constructed the MRP and participated in data collection during SHEBA, as did James Pinto (University of Colorado). We appreciate the many suggestions offered by Richard Moritz (University of Washington) to improve the quality of this paper. Finally, we acknowledge the invaluable assistance provided by the crew of the Des Groseilliers and the SHEBA logistics support team.

References

Claffey, K. J., E. L. Andreas, D. K. Perovich, C. W. Fairall, P. S. Guest, and O. Persson, Surface temperature measurements at SHEBA, in *Fifth Conference on Polar Meteorology and Oceanography*, pp. 327–332, Am. Meteorol. Soc., Boston, Mass., 10–15 Jan. 1999.

Curry, J. A., et al., FIRE Arctic clouds experiment, *Bull. Am. Meteorol. Soc.*, *81*(1), 5–29, 2000.

Davis, J. C., *Statistics and Data Analysis in Geology*, 2nd ed., 646 pp., John Wiley, Hoboken, N. J., 1986.

Key, J., and A. J. Schweiger, Tools for atmospheric radiative transfer: Streamer and FluxNet, *Comp. Geosci.*, *24*(5), 443–451, 1998.

Key, J., J. B. Collins, C. Fowler, and R. S. Stone, High-latitude surface temperature estimates from thermal satellite data, *Remote Sens. Environ.*, *61*, 302–309, 1997.

Lindsay, R. W., and D. A. Rothrock, Arctic sea ice surface temperature from AVHRR, *J. Clim.*, *7*, 174–183, 1994.

Lindsay, R. W., D. B. Percival, and D. A. Rothrock, The discrete wavelet transform and the scale analysis of the surface properties of sea ice, *IEEE Trans. Geosci. Remote Sens.*, *34*, 771–787, 1996.

Liou, K., *An Introduction to Atmospheric Radiation*, 392 pp., Academic, San Diego, Calif., 1980.

Maslanik, J., R. Stone, J. Pinto, J. Wendell, and C. Fowler, Mobile-platform observations of surface energy budget parameters at the SHEBA site, in *Fifth Conference on Polar Meteorology and Oceanography*, pp. 128–131, Am. Meteorol. Soc., Boston, Mass., 10–15 Jan. 1999.

Maslanik, J., J. Key, C. W. Fowler, T. Nguyen, and X. Wang, Spatial and temporal variability of satellite-derived cloud and surface characteristics during FIRE-ACE, *J. Geophys. Res.*, *106*, 15,233–15,250, 2001.

Muller, F., H. Blatter, and G. Kappenberger, Temperature measurement of ice and water surfaces in the north water area using an airborne radiation thermometer, *J. Glaciol.*, *15*(73), 241–250, 1975.

Pegau, W. S., and C. A. Paulson, The role of summer leads in the heat and mass balance of the upper Arctic Ocean, in *Fifth Conference on Polar Meteorology and Oceanography*, pp. 401–403, Am. Meteorol. Soc., Boston, Mass., 10–15 Jan. 1999.

Perovich, D. K., et al., Year on ice gives climate insights, *Eos Trans. AGU*, *80*, 481, 1999.

Research Aviation Facility (RAF), The NCA/NSF EC-130Q Hercules (N130AR): Overview and Summary of Capabilities, *RAF Tech. Bull. 3*, Natl. Cent. for Atmos. Res., Boulder, Colo., 1994.

Salisbury, J. W., D. M. D'Aria, and A. Wald, Measurements of thermal infrared spectral reflectance of frost, snow, and ice, *J. Geophys. Res.*, *99*, 24,235–24,240, 1994.

Steffen, K., and J. E. Lewis, Technical note: Surface temperatures and sea ice typing for northern Baffin Bay, *Int. J. Remote Sens.*, *9*(3), 409–422, 1988.

J. Curry, School of Earth and Atmospheric Sciences, Georgia Institute of Technology, 311 Ferst Drive, Atlanta, GA 30332-0340, USA. (curryja@eas.gatech.edu)

J. A. Haggerty, National Center for Atmospheric Research, P.O. Box 3000, Boulder, CO 80307, USA. (haggerty@ucar.edu)

J. Maslanik, Department of Aerospace Engineering Sciences, 429 UCB, University of Colorado, Boulder, CO 80309-0429, USA. (james.maslanik@colorado.edu)